ELSEVIER

Nuclear Physics A 683 (2001) 21–47

NUCLEAR PHYSICS A

www.elsevier.nl/locate/npe

Transition probabilities in negative parity bands of the ^{119}I nucleus

J. Srebrny [a,*], Ch. Droste [a], T. Morek [a], K. Starosta [a], A.A. Wasilewski [b], A.A. Pasternak [c], E.O. Podsvirova [c], Yu.N. Lobach [d], G.H. Hagemann [e], S. Juutinen [f], M. Piiparinen [f], S. Törmänen [f], A. Virtanen [f]

[a] *Nuclear Physics Division, IEP, Warsaw University, Hoża 69, 00-681 Warsaw, Poland*
[b] *Institute for Nuclear Studies, 05-400 Świerk, Poland*
[c] *A.F. Ioffe Physical Technical Institute RAS, ul. Politekhnicheskaja 26, 194021 St.-Petersburg, Russia*
[d] *Institute for Nuclear Research UAS, pr. Nauki 47, 252028 Kiev, Ukraine*
[e] *The Niels Bohr Institute, Blegdamsvej 17, DK-2100 Copenhagen, Denmark*
[f] *Department of Physics, University of Jyväskylä, PO Box 35, FIN-40351 Jyväskylä, Finland*

Received 21 October 1999; revised 3 August 2000; accepted 8 September 2000

Abstract

Lifetimes in four negative-parity bands of ^{119}I were measured using DSAM and RDM. ^{119}I nuclei were produced in the ^{109}Ag(^{13}C,3n) reaction, $\gamma\gamma$ coincidences were collected using the NORDBALL array. RDDSA — a new method of RDM analysis — is described. This method allowed for the self-calibration of stopping power. From 31 measured lifetimes, 39 values of B(E2) were established. Calculations in the frame of the Core Quasi Particle Coupling (CQPC) model were focused on the problem of susceptibility of the nucleus to γ-deformation. It was established that nonaxial quadrupole deformation of ^{119}I plays on important role. The Wilets–Jean model of a γ-soft nucleus describes the ^{119}I nucleus in a more consistent way then the Davydov–Filippov model of a γ-rigid nucleus.

Keywords: NUCLEAR REACTION ^{109}Ag(^{13}C,3n) $E = 54$ MeV, side-feeding time; Nuclear spectroscopy measured $E\gamma$, $I\gamma$, $\gamma\gamma$-coincidence, DSA, RDM; ^{119}I levels deduced $T_{1/2}$, B(E2); Recoil distance Doppler shift attenuation methods, deduced stopping power; Quadrupole nonaxial deformation, γ-softness

1. Introduction

In the previous study of the ^{119}I nucleus [1], 15 bands were found. They reflect many ways of nuclear excitation, including one-, three- and five-quasiparticle structures, quasi-gamma bands and band terminations. The group of four negative-parity bands

* Corresponding author.
E-mail address: js@npdaxp.fuw.edu.pl (J. Srebrny).

0375-9474/01/$ – see front matter
PII: S0375-9474(00)00457-7

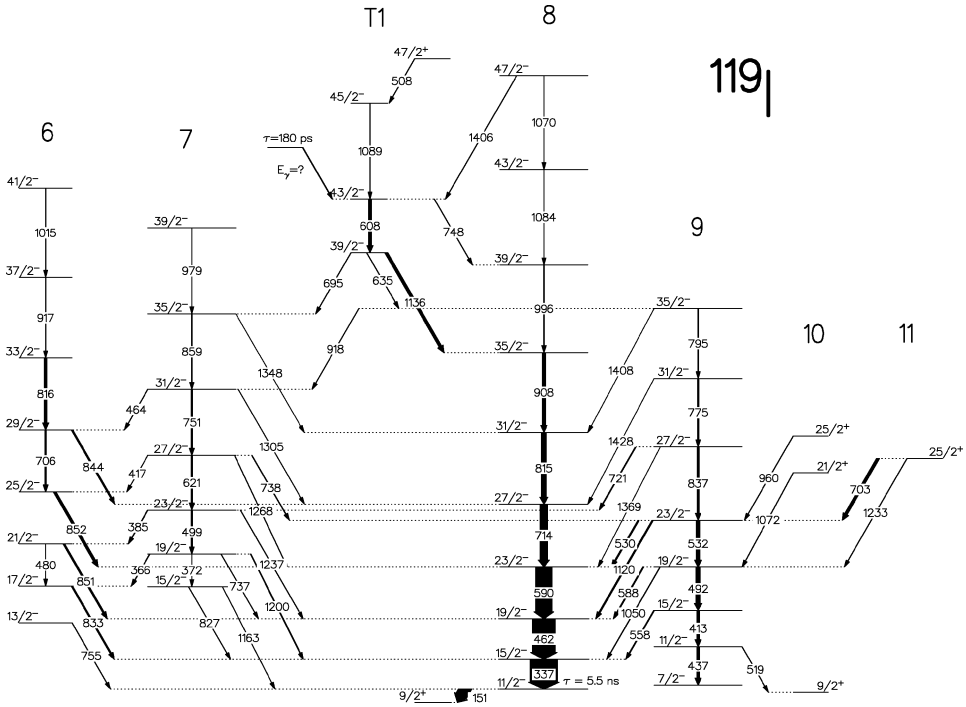

Fig. 1. Partial level scheme of the ^{119}I nucleus [1]. Only levels discussed in the present paper are shown.

(6–9 in Fig. 1) can be interpreted as resulting from a $h_{11/2}$ quasiproton coupled to an axially asymmetric core. The similarity of the energies of bands 7 and 8 in ^{119}I to the ground state and quasi-gamma bands in ^{120}Xe supports this interpretation. To test the importance of nonaxial quadrupole deformation, lifetime measurements, using Doppler recoil distance and Doppler shift attenuation methods, have been undertaken.

In the RDM experiment, which was performed with a relatively thick target, the analysis proposed by Pasternak [2] was carried on. Instead of the decay curves, lineshapes at different target–stopper distances were analysed using the program for the DSA method. The name Recoil Distance Doppler Shift Attenuation Method (RDDSAM) has been proposed for such analysis. Special treatment of the determination of stopping power and side-feeding time is described in Section 2. The influence of the deorientation effect on the accuracy of lifetimes measured by RDM is discussed in Appendix A. A detailed presentation of γ-lineshape analysis and lifetime evaluation is given in Section 3.

The analysis of experimental data gave lifetimes for 31 excited states in ^{119}I. It gives together with results of [1] a very good basis for a theoretical study of the quadrupole collectivity in ^{119}I. Within the framework of the Core Quasi Particle Coupling (CQPC) model, the influence of β- and γ-deformation of the core on the energy levels and B(E2) transition probabilities were studied. In particular, the susceptibility of the nucleus to γ-deformation was investigated. The problem whether nuclei in the $50 < Z, N < 82$ region are γ-soft or

γ-rigid has been studied for many years [3–6]. The results of our theoretical calculations are given in Sections 4 and 5.

2. Experimental

The experiment was performed at the Tandem Accelerator Laboratory of the Niels Bohr Institute. The excited states of ^{119}I were populated via the ^{109}Ag(^{13}C,3n) reaction at a beam energy of 54 MeV. Two kinds of lifetime measurements were performed. The Doppler Shift Attenuation Method (DSAM) was applied with a thick self-supported target of 5.7 mg/cm^2. In the other measurement, the Recoil Distance Method (RDM) with thin targets of 0.69 and 0.82 mg/cm^2 was used. In this case, a plunger device was installed inside the detector array. The RDM-experiment was performed at 16 target–stopper distances, namely 15, 22, 29, 37, 42, 52, 72, 92, 4022 and 8022 μm for the 0.82 mg/cm^2 thick target and for 122, 222, 322, 522, 1022 and 2022 μm for the 0.69 mg/cm^2 thick target. As a stopper 6.3 mg/cm^2 Au foil was used. The $\gamma\gamma$ coincidences were collected with the NORDBALL detector array [1], consisting of 20 Compton-suppressed Ge detectors placed at four different rings at angles of 37°, 79°, 101° and 143° relative to beam direction. The distance between detectors and target was equal to 17.7 cm. The coincidence spectra gated on transitions below the transition of interest and the sums of these gated spectra were analyzed. In several cases, spectra gated on transitions above the one of interest were used. The γ-lines measured at 37° and 143° were used for the DSAM analysis.

2.1. Method of data analysis

The analysis of experimental lineshapes was carried out using an updated version of the package of computer codes COMPA, GAMMA and SHAPE [7] for both the DSAM and RDM data. A detailed description of codes and methods of analysis is given in [8]. Here we show only the important points, different from those used by other authors, particularly the self-calibration of stopping power and estimation of statistical side-feeding time.

For the RDM data lineshapes from all sensitive distances were analyzed simultaneously. In the RDDSA method applied here for data analysis, shifted and unshifted peaks are regarded as components of one γ-line. It is therefore possible to obtain a reliable lifetime value even for cases when the components overlap. For a low-energy γ-line, where the two components are not resolved, and for cases where the target thickness is comparable with the range of the recoils, we found the use of the RDDSA method necessary. The lifetimes of the investigated levels where determined by a best fit to the experimental lineshapes of the γ-transitions. In Section 3, for many of the analysed transitions the experimental points, fitted lineshapes and χ^2 curves are presented. In our paper, χ^2 signifies standard χ^2 value divided by the number of degrees of freedom (*NDF*). *NDF* was from 15 to 30 for the DSA data and ≈ 60 (in one case 200) for the RDDSA data. The statistical error of the lifetime was determined from the value of $\chi^2(\min) + \Delta\chi^2$, where

$$\Delta\chi^2 = \chi^2(\min)/NDF. \tag{1}$$

All other uncertainties have been included in a less precise way. Through many trials we had found how they influenced the final results and increased the final errors accordingly. These main uncertainties, included in an unstatistical way, were the following:

(a) the errors of intensity of feeding transitions,
(b) the errors of lifetime of feeding transitions,
(c) background under the fitted γ-line,
(d) the errors of coefficients of the stopping power formula,
(e) the errors of τ_{sf} — statistical cascade side-feeding time.

In some cases where all above factors play the important role, instead of formula (1) the following very conservative semiempirical formula was used:

$$\Delta\chi^2 = 0.2\chi^2 \text{ (min)}. \tag{2}$$

It was evaluated that the deorientation effect should not influence the presented results more than $2 \div 3\%$ (see Appendix A). Additionally, we checked that for the two strongest transitions, 337 keV ($\tau \approx 45$ ps) and 462 keV ($\tau \approx 8$ ps), total intensity (stop + flight components) normalized to intensity of the 151 keV transition did not alter significantly for distances from 15 μ to 2000 μ.

2.2. Determination of stopping power parameters.

The slowing-down process is approximated by the following expression [8–10]:

$$\mathrm{d}\epsilon/\mathrm{d}\rho = f_{\mathrm{e}} k \epsilon^{1/2} + f_{\mathrm{n}} \epsilon^{1/2}/(0.67\varphi_{\mathrm{n}} + 2.07\epsilon), \tag{3}$$

where ϵ and ρ are the energy and the range in Lindhard units respectively; k is the Lindhard electronic stopping power coefficient; f_{e} and f_{n} are correction factors of the Lindhard cross sections [11] for the electronic and nuclear stopping power, respectively; φ_{n} is an additional correction factor of the nuclear stopping power calculated from LSS-theory [12]. This simple approximation of LSS with $\varphi_{\mathrm{n}} = 1$ is close to that proposed in [10].

In the presented RDM experiment, the target thicknesses were close to the recoil range, causing part of the recoils to be stopped inside the target. As a result, the peak shape is influenced by the slowing-down process of recoils. Therefore, the determination of the stopping power parameters is an important task not only as usual for the DSA experiment, but also for the RDM experiment. For the recoils escaping from the target to the vacuum, the calculation is performed in the same way as in the DSA method and the vacuum is regarded as an additional material (target,vacuum and stopper). In our experiments the same target material, ^{109}Ag, was used for both thick and thin targets. This gave a good opportunity for self-calibration of stopping power parameters and improved the accuracy of the DSA and RDDSA lifetime measurements. The correction factors of stopping power (Eq. (3)) were determined by the "*semithick target*" method [8,9,13–15]. This was done by analysis of the lineshape of the γ-rays emitted by recoils moving in the vacuum after they escape the target. The following conditions have to be fulfilled for the use of this method:

(a) target thickness is comparable with the range of recoils,

(b) the characteristic time τ_{sp} for stopping of recoils in the target is much shorter than the lifetime τ of the nuclear state,
(c) time of flight of the recoils in the vacuum is much longer than τ.

Under such conditions, the lineshape (including γ's emitted in vacuum) is fully determined by the slowing-down and multiple scattering of recoils in the target, assuming that the kinematics of the nuclear reaction and target thickness are well defined. In the present work, a "*semithick target*" of 0.82 mg/cm^2 was used for the RDM-experiment at large distances between the target and stopper. The most intense γ-lines, 337 keV ($\tau \approx 45$ ps) and 462 keV ($\tau \approx 8$ ps) in the spectrum gated on the 590 keV transition, were analyzed at a distance of 8022 μm.

The value of the correction factor for electronic stopping power was determined to be $f_e = 1.27 \pm 0.07$ [8]. That values is in good agreement with the one obtained by a similar method for stopping Cd recoils in a Cd target ($f_e = 1.28 \pm 0.10$) [7] and In in Mo ($f_e = 1.30 \pm 0.15$) [16]. The electronic stopping power parameter ($f_e = 1.36 \pm 0.11$) measured directly for I ions in Ag [17] agrees with our result.

The correction factors of nuclear stopping power were determined for two different cases:

(a) $f_n = \varphi_n$, then we obtained $f_n = \varphi_n = 0.70 \pm 0.07$ which agrees with the case of Cd in Cd (0.62 ± 0.06) [9],
(b) $\varphi_n = 1$, then $f_n = 0.77 \pm 0.07$ was obtained.

Both sets of correction factors gave a similarly good description of the shape of γ-lines emitted in a vacuum. The universal nuclear stopping power given by Ziegler et al. [18] for the energy range $0.1 \leqslant \epsilon^{1/2} \leqslant 2$ can be approximated for case (a) as $f_n = \varphi_n = 0.75$ and for case (b) as $f_n = 0.82$.

Energy losses in stopper material (Au) were included in calculation. The stopping power for the stopper was obtained from the shape of the long-lived γ-line taken at small distances.

2.3. Determination of side-feeding time

The proper correction of lifetime for side-feeding time (τ_{sf}) is the most difficult problem of the DSA method. In Fig. 2, the entry state distribution derived for conditions of our experiment from the Monte Carlo calculation by the program COMPA is shown. At high spins, close to the edge of entry state "cloud", side-feeding time should be short ($\leqslant 0.05$ ps) and determined mainly by fast statistical dipole transitions. As spin of investigated states decreases, τ_{sf} should become larger due to the influence of longer stretched cascades, which take off the excess of angular momentum. We propose a simple empirical formula taking into account dependence of τ_{sf} (ps) on level energy E_{lev} (MeV) with spin I_{lev} ($\hbar$):

$$\tau_{sf}(E_{lev}, I_{lev}) \approx 0.007\{E_{entry}(I_{lev}) - E_{lev}\} + 0.007(I_{max} - I_{lev}), \quad (4)$$

where I_{max} is the spin value above which the influence of stretched cascades is negligible and $E_{entry}(I_{lev})$ is the energy of the entry line for $I = I_{lev}$. We determine I_{max} as spin at which the horizontal line, starting from the center of the entry state distribution, crosses

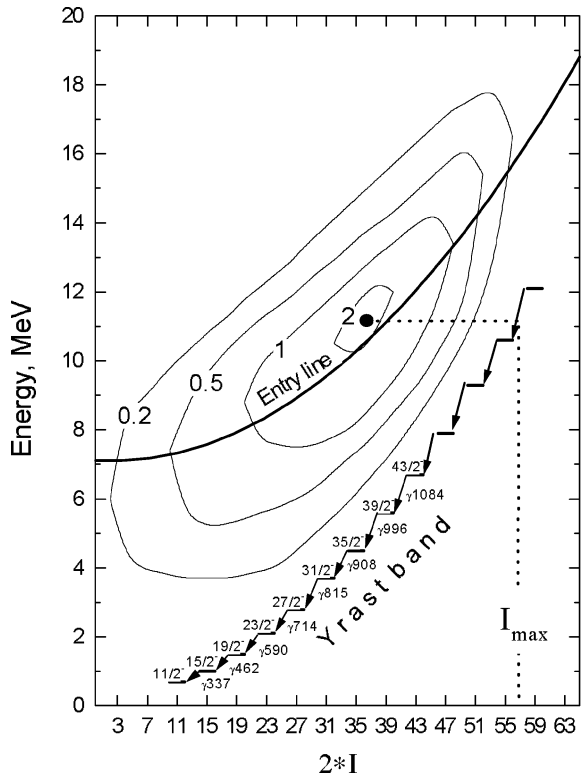

Fig. 2. Entry state population for the reaction ^{109}Ag(^{13}C,3n)^{119}I at bombarding energy 54 MeV. The cross section is given in mb/(MeV $\hbar$) units. Entry line, being the centre of gravity of entry state population for each spin value is also shown.

the yrast line. The first part of this formula reflects contribution of the "vertical" dipole statistical transitions to τ_{sf}. Such linear dependence of τ_{sf} on E_{lev} was previously reported in many works [8,13,19], where compound nuclear reactions with rather low input angular momentum (α-particle induced reactions, HI reactions with ions up to oxygen and energy not far from the Coulomb barrier) were studied. The second part of Eq. (4), introduced by us, reflects the contribution of stretched cascades on the way from entry states to the investigated level.

We have checked this formula in cases where single strong γ-lines correspond to short-lived transitions. Then, precise analysis of the lineshape [7,8,15] allows the measurement of τ_{sf}. In ^{119}I [8], values of τ_{sf} derived from the DSA analysis of γ-lines, corresponding to yrast transitions from $39/2$, $35/2$ and $31/2$ states of band 8, are equal to 0.10(3) ps, 0.13(4) and 0.14(5) ps. For the ^{111}Cd(^{12}C,3n)^{120}Xe reaction, which is similar to the one used by us, the center of the entry state distribution is located near $I \approx 12$ (mainly due to the thick target) and a $\tau_{sf} = 0.040 \pm 0.015$ ps for 18^+ yrast state was measured [21]. The experimental values obtained in both reactions are in good agreement with ones calculated using Eq. (4). Moreover, we have checked this formula for other reactions [13,15,19,20] and also recived good results.

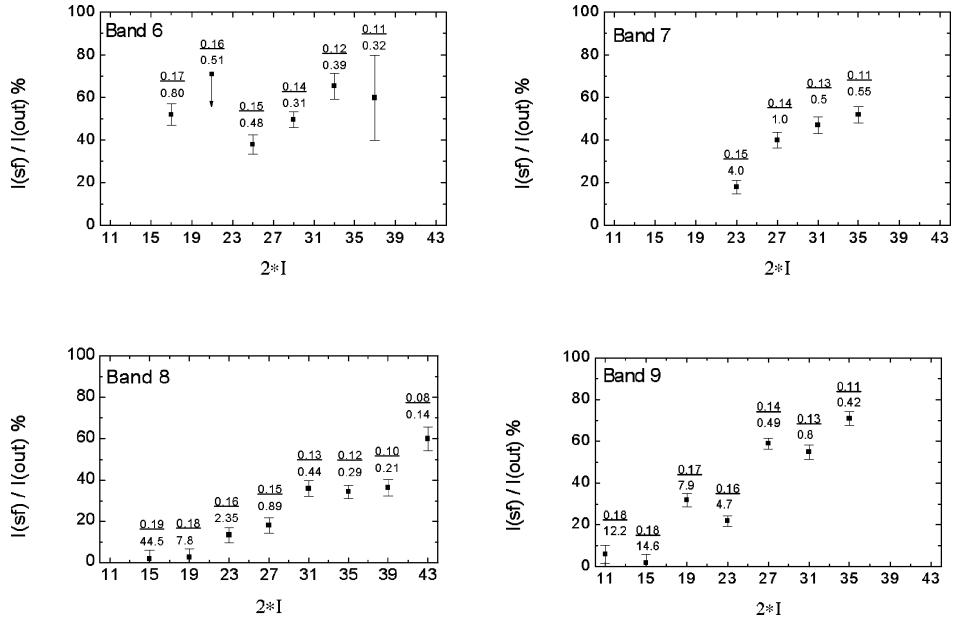

Fig. 3. Side-feeding intensity normalized to total outgoing intensity for each measured level in bands 6–9. The value of τ_{sf} evaluated by Eq. (4) is given in numerator over each experimental point. The assigned lifetime (see Tables 1 and 2) is given in denominator.

Side-feeding time τ_{sf} compared with τ of the investigated level and relative side-feeding intensities are presented in Fig. 3. We suppose that the typical error of τ_{sf} evaluated by (Eq. (4)) is about 25%, the same as errors of τ_{sf} calculated in [8]. Since measured and calculated τ_{sf} are smaller than τ of investigated levels, our results of lifetime measurements are practically independent from details of the side-feeding pattern. In our case, the measurements of τ_{sf} for the yrast $39/2$, $35/2$ and $31/2$ levels ruled out the frequently used assumption [22] that τ_{sf} of unobserved feeding is similar to the observed effective discrete feeding time of the state of interest (see Fig. 1 and Tables 1 and 2).

2.4. $D_\circ$-determination

Usually the determination of a systematic shift of the measured target–stopper distance $D_\circ$ is based on the decay curve, regarding $D_\circ$ as a variable parameter. In the present work this was achieved by the RDDSA analysis of the $\gamma 590$ and $\gamma 462$ lineshapes performed for distances 15, 22, 29, 37, 42 and 52 μm. These γ-lines are the most intense among the relatively short-living ones ($\tau \approx 2.5$ ps and ≈ 8 ps, respectively), therefore they can be used for precise determination of $D_\circ$ value. Lineshape calculations were made for three cases: $D_\circ = 2.5$, 5.0 and 7.5 μm. In each case χ^2-curves were determined, then summed for six target–stopper distances (as shown on the upper part of Fig. 4). Finally, the χ^2-curves for $\gamma 590$ and $\gamma 462$ were summed and fitted by a parabola near the minimum (as shown on bottom right). $D_\circ = 5.7 \pm 0.3$ μm was determined on the basis of this χ^2-dependence. The dependence of lifetime on $D_\circ$ for $\gamma 590$ is shown in Fig. 4 (bottom left). The error of life-

Table 1
Lifetimes in bands 8, 9 and T1. Band numbering according to Fig. 1 and Ref. [1]

Band	J_i	E_γ (keV)[a]	τ (ps)[b]	Angles	Gate[c]	Dist. (μm)
8	$15/2^-$	337	44.5 ± 3.0^R	143°	590	22,72,92 122,322,1022
8	$19/2^-$	462	7.8 ± 0.7^R	143°	590	15,22,29, 37,42,52
8	$23/2^-$	590	2.35 ± 0.30[d]	143°, 37°	462	15,22,29
8	$27/2^-$	714	0.89 ± 0.15^D	143°, 37°	g2	
8	$31/2^-$	814.6	0.44 ± 0.08^D	143°, 37°	g2	
8	$35/2^-$	908	0.29 ± 0.04^D	143°, 37°	g2	
8	$39/2^-$	996	0.21 ± 0.04^D	143°, 37°	g2	
8	$43/2^-$	1084	0.14 ± 0.06^D	143°, 37°	g2	
T1	$39/2^-$	1136	1.9 ± 1.0^R	143°	g2,g4	15,22,29
T1	[e]	608;1136	180 ± 40^R	143°	g2,g4	122,222, 322,522
T1	$43/2^-$	608	4.7 ± 1.5^R	143°	g2	15,22,29,72
T1	$45/2^-$	1089	$0.22^{+0.16}_{-0.13}{}^D$	143°		
9	$11/2^-$	437;519	12.2 ± 2.4^R	143°	413	92,122
9	$15/2^-$	413	14.6 ± 1.8^R	143°	492	52,92.122
9	$19/2^-$	492	7.9 ± 0.9^R	143°	g3	29,37,52
9	$23/2^-$	1120	4.7 ± 0.8^R	143°	g2	15,22,29,42
9	$27/2^-$	837	0.49 ± 0.11^D	143°	g2	
9	$31/2^-$	775	$0.8^{+0.4}_{-0.2}{}^D$	143°	g2	
9	$35/2^-$	795	0.42 ± 0.06^D	143°, 37°	g2	

[a] E_γ — energy of γ-transition used for lifetime determination.
[b] Method of measurement and data evaluation: R — RDDSA, D — DSA.
[c] Gates (keV): g2 = 337 + 462, g3 = 337 + 462 + 590, g4 = 337 + 462 + 590 + 714.
[d] Adopted value, $\tau^{DSA} = 2.2 \pm 0.4$ ps, $\tau^{RDDSA} = 2.5 \pm 0.4$ ps.
[e] Lifetime of the long-lived component feeding level $43/2^-$.

time due to uncertainty of $D_\circ$ is about 0.1 ps. The value of $D_\circ = 5.7 \pm 0.3\,\mu$ was used to correct all measured target–stopper distances.

3. Discussion of experimental results

The final τ values are shown in Tables 1 and 2. Corresponding B(E2) values are presented in Fig. 5.

The main points of the lifetime analysis are given below for all bands. The figures present typical examples of γ-lineshape analysis. In many cases, the relative intensities of the transitions, taken from [1], have been used as fixed parameters.

Table 2
Lifetimes in bands 6 and 7. Band numbering according to Fig. 1 and Ref. [1]

Band	J_i	E_γ (keV)[a]	τ (ps)[b]	Angles	Gate[c]	Dist. (μm)
6	$17/2^-$	833	$0.8^{+0.4}_{-0.3}{}^{D}$	143°	g2	
6	$21/2^-$	480	$0.51^{+0.17}_{-0.13}{}^{D}$	143°	337	
6	$25/2^-$	851.8	0.48 ± 0.15^{D}	143°,37°	462,g2	
6	$29/2^-$	844	0.31 ± 0.10^{D}	143°,37°	g3	
6	$33/2^-$	815.6	$0.39^{+0.13}_{-0.08}{}^{D}$	143°,37°	g2,g3	
6	$37/2^-$	917.2	$0.32^{+0.16}_{-0.12}{}^{D}$	143°,37°	g3	
6	$41/2^-$	1015	0.36 ± 0.06^{D}	143°,37°	g3	
7	$23/2^-$	1237	4 ± 1^{R}	143°	g3	15,22,29,42
7	$27/2^-$	621	1.00 ± 0.25^{D}	143°,37°	g2	
7	$31/2^-$	751	0.50 ± 0.15^{D}	143°,37°	g2	
7	$35/2^-$	859	0.55 ± 0.14^{D}	143°,37°	g2	
11	$25/2^+$	1233	9.5 ± 2.5^{R}	143°	g2	15,22,29,42

[a] E_γ — energy of the γ-transition used for lifetime determination.
[b] Method of measurement and data evaluation: R — RDDSA, D — DSA.
[c] Gates (keV): g2 = 337 + 462, g3 = 337 + 462 + 590.

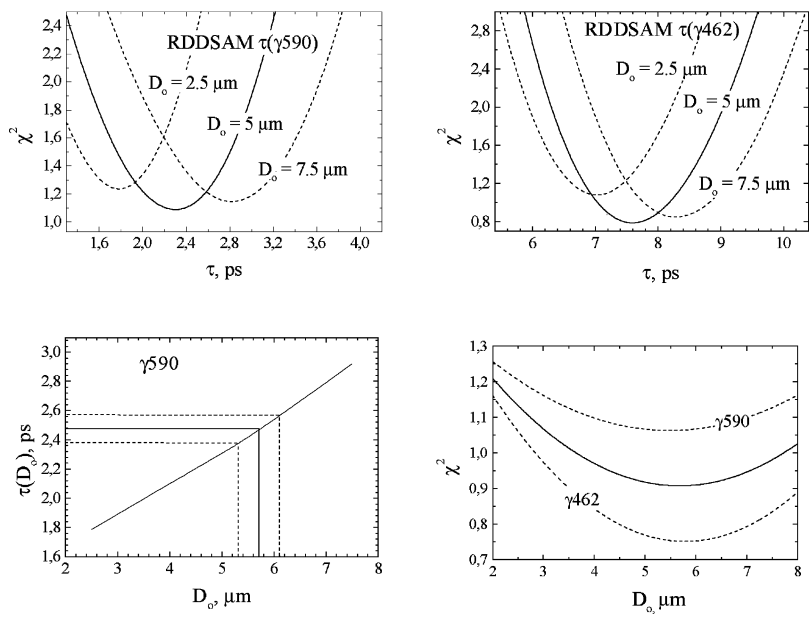

Fig. 4. Determination of $D_\circ$, the systematic shift of measured target–stopper distance. Upper panels show $\chi^2(\tau)$ curves for various $D_\circ$ values. Lower left panel shows the dependence of $\tau(23/2^-)$ level in band 8 on $D_\circ$, lower right — χ^2 curves for final $D_\circ$ determination.

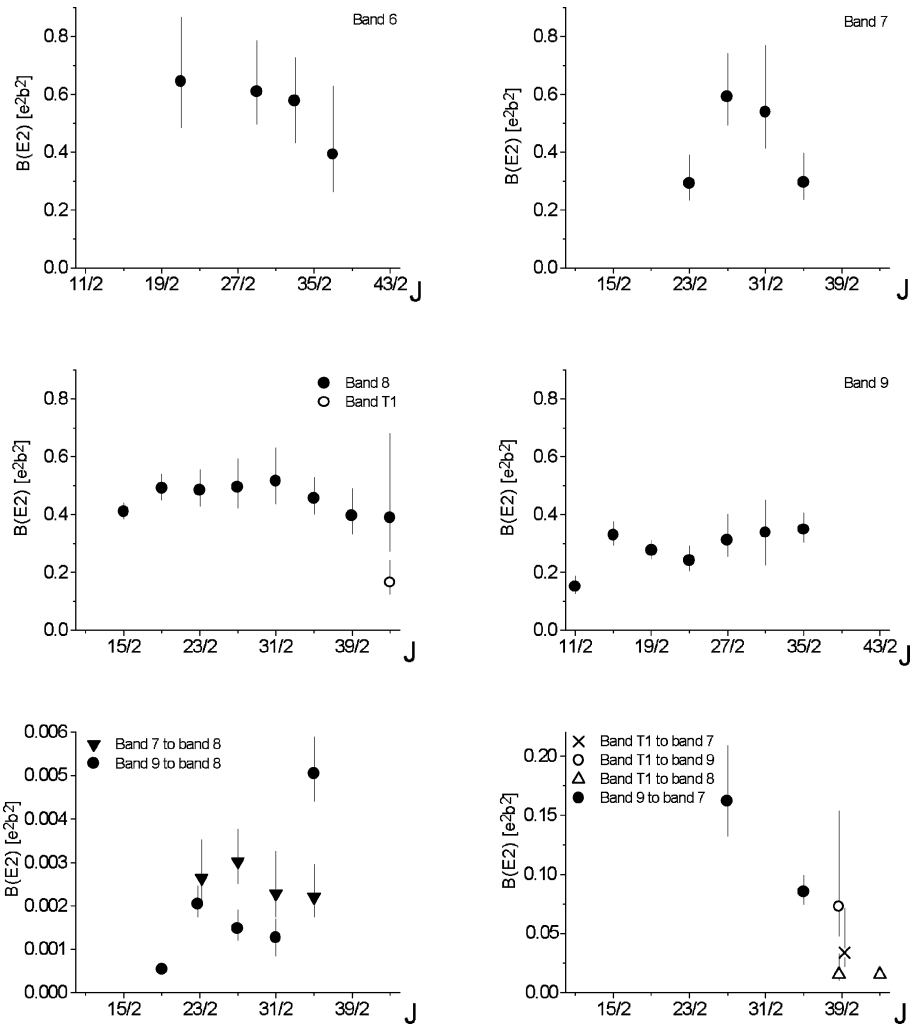

Fig. 5. B(E2) values corresponding to measured lifetimes in the ^{119}I nucleus. Bottom figures show B(E2) of the interband transitions.

3.1. Band 8

In this band, the lifetime values for the 5 upper levels (from $43/2^-$ to $27/2^-$) were obtained from DSA analysis. Lifetimes of levels $19/2^-$ and $15/2^-$ were obtained by RDDSAM from spectra gated on the 590 keV transition (Fig. 6).

Level $43/2^-$. Lifetime of this level was obtained from the simultaneous analysis of $\gamma 1084$ and $\gamma 1089$ (band T1). The lifetime error includes the uncertainity of the side-feeding time estimation (see Section 2.3).

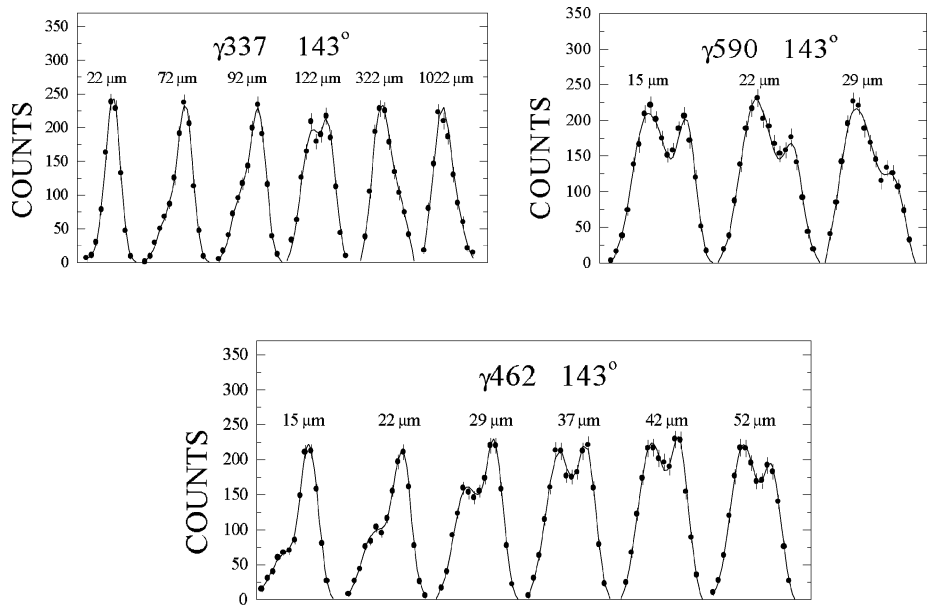

Fig. 6. RDDSA analysis of γ-lineshapes of 337, 462 and 590 keV γ-lines in band 8 at different target–stopper distances. Experimental data points (0.5 keV/chanel) are shown after background subtraction.

Level $39/2^-$. The lifetime of this level was determined from the 996 keV transition (Fig. 7).

Level $35/2^-$. One can see in Fig. 7 that in the spectrum collected at 37° the contamination of $\gamma 908$ by $\gamma 905.3$ (probably from band 11) has only a small influence on $\tau(\gamma 908)$. In the analysis of the spectrum observed at 143°, we used the known relative intensity of $\gamma 905.3$ and its $\tau \geqslant 2$ ps (determined from the narrow lineshape in 37° data). It was possible to obtain $\tau(\gamma 908)$ for both angles and they agree with each other.

Level $31/2^-$. The transition of 814.6 keV, used for lifetime determination, overlaps with $\gamma 815.6$ from band 6. The positions of both peaks and their intensity ratio $I(815.6)/I(814.6) = 0.22$, were used in the analysis shown in Fig. 8.

Level $27/2^-$. The $\gamma 714$ used for lifetime determination is a member of the complex multiplet also consisting of $\gamma 721(27/2^- \to 23/2^-$, bands 9–7), $\gamma 706(29/2^- \to 25/2^-$, band 6) and $\gamma 703(25/2^+ \to 23/2^-$, bands 11–9). The lifetime of $\tau(\gamma 714)$ was obtained from spectra taken at both angles. The procedure of step-by-step subtraction was used.

3.2. Bands 9 and 11

Level $31/2^-$. The τ value of this level was determined from the DSA lineshape analysis of $\gamma 775$ at 143° only, and therefore has a relatively large error. At 37° the 775 keV line

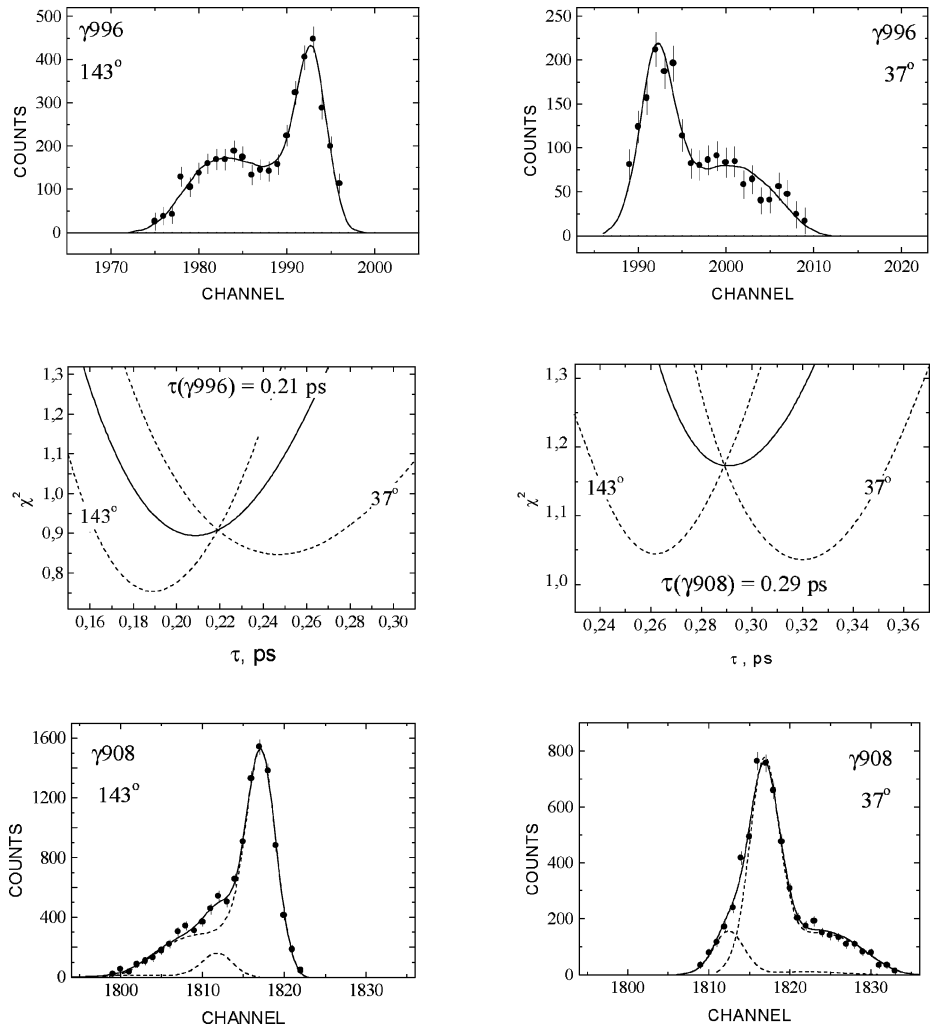

Fig. 7. DSA lineshape analysis of the 908 and 996 keV lines in band 8. Experimental spectra (0.5 keV/channel) are presented after background subtraction, dashed lines show components of the analysed multiplets. In χ^2 plots, dashed lines correspond to χ^2 values for each detector angle. Thick lines correspond to total χ^2, summed over data from both angles. Total NDF taking into account data for both angles is used to get total χ^2.

overlaps with the 780 keV line from band 11 and a few other background lines. The second gamma transition depopulating this level, $\gamma 1428$, has very low intensity.

Level $27/2^-$. The lifetime of this level was determined by analysis of $\gamma 837$, a member of the complex multiplet: 833, 837, 844, 852, 859 keV. The spectrum taken at 143° gated on the 462 keV line was used because in this gate the contamination by $\gamma 833$ is absent.

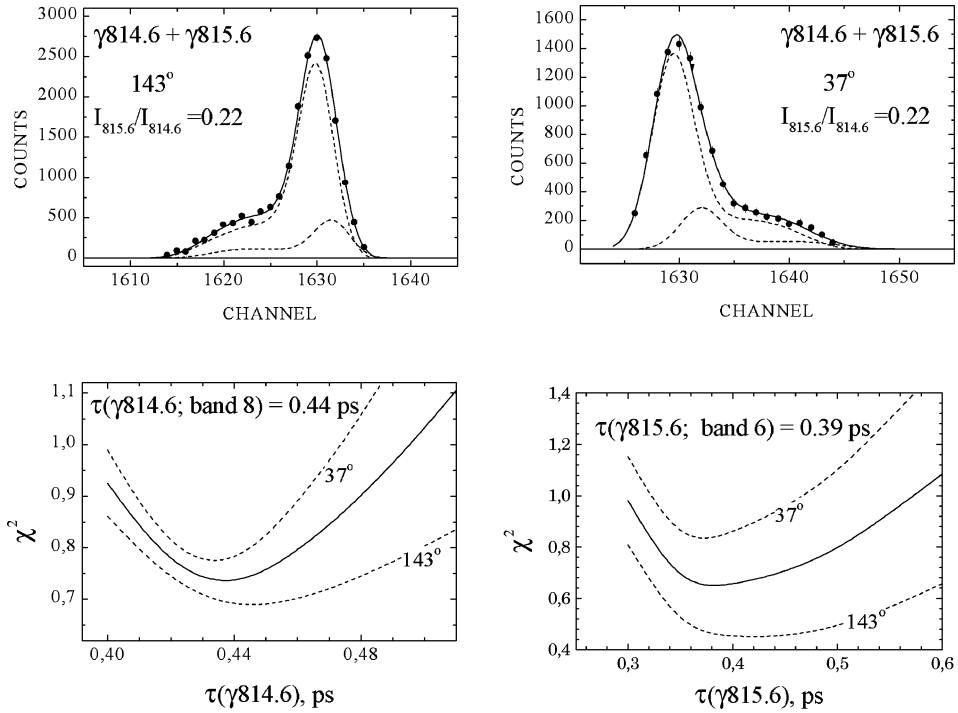

Fig. 8. DSA lineshape analysis of the close-lying 814.6 keV and 815.6 keV γ lines. Lower left panel shows χ^2 for fixed value of τ(815.6 keV) and lower right χ^2 for fixed value of τ (814.6). See caption of Fig. 7.

Level $23/2^-$ (band 9) and $25/2^+$ (band 11). The first of these levels decays by three γ-transitions: 530, 532 and 1120 keV. From the lineshape of $\gamma 1120$ it was estimated (DSA) that the lifetime of this level is greater than 2 ps. More detailed RDDSA analysis was performed using $\gamma 1120$ observed in the sum of spectra taken at 143° gated on the 337 keV and 462 keV lines. Note that this level is fed from band 11 (level $25/2^+$) by the 703 keV E1-transition, therefore the RDDSA analysis of $\gamma 1120$ was performed taking into account that $\tau(25/2^+; \gamma 1233) = 9.5 \pm 2.5$ ps, which gave $\tau(23/2^-; \gamma 1120) = 4.7 \pm 0.8$ ps.

Level $15/2^-$. Gate 492 keV was used for RDDSA analysis of $\gamma 413$ at three distances: 52, 92, 122 μm; the result is shown in Fig. 9.

3.3. Band 7

Level $31/2^-$. $\gamma 751$, which was used to establish the lifetime of this level by DSAM, is situated in the complex background region. In the spectrum taken at 143°, the shifted component of $\gamma 751$ overlaps with three small γ-peaks on the lower-energy side, making the determination of $\tau(\gamma 751)$ at this angle very difficult. At 37° the influence of these three peaks on the lineshape of $\gamma 751$ is negligible and it was thus possible to perform an analysis

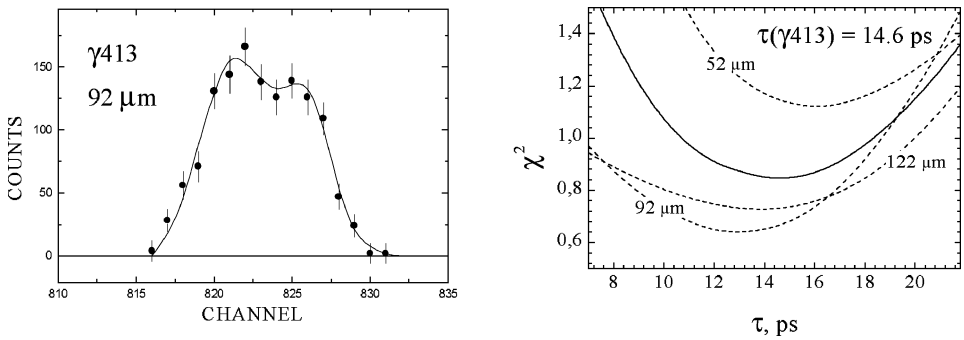

Fig. 9. RDDSA analysis of the 413 keV γ-line of band 9. Experimental γ-spectrum (0.5 keV/channel) after background subtraction is presented in the left panel. In the χ^2 plot, dashed lines correspond to χ^2 value for each target–stopper distance. Those χ^2 plots, shown for illustration only, are not used separately for lifetime determination. Total χ^2, beeing a sum over data for all distances, was calculated using total NDF. Lifetime was determined from total χ^2 (thick line).

of $\gamma 751$ and $\gamma 755$ simultaneously taking into account the estimation of $\tau(\gamma 755) \geqslant 2$ ps from the analysis of the spectrum taken at 143°.

Level $27/2^-$. The lifetime of this level was obtained from DSA analysis of $\gamma 621$. There are small background peaks both from the left and right. The number of channels in the area sensitive for fitted parameters uncontaminated by background peaks was sufficient for lineshape analysis. Because of the difference between lifetime values obtained from spectra taken at 37° and 143° an error of 25% was adopted.

Level $23/2^-$. The lifetime of this level was obtained from simultanous RDDSA analysis of $\gamma 1237$ and $\gamma 1233$ (decays from the $25/2^+$ state in band 11) in the spectrum taken at 143°.

3.4. Band 6

All 7 lifetimes were obtained by DSA analysis of lineshape of weak or close-lying lines. Because of this, in most of the cases the relatively large errors are quoted in Table 2.

3.5. Band T1

In RDDSA analysis, a long-lived 40% component of the 608 keV line was found in the decay of level $43/2^-$ to level $39/2^-$. A similar long-lived 30% component of the 1136 keV line was observed in the decay of level $39/2^-$ to level $35/2^-$. These observations can be explained only by the existence of long-lived level ($\tau = 180 \pm 40$ ps) feeding level $43/2^-$. The intensity of the transition connecting the long-lived level with level $43/2^-$ should be about 1.7% of the intensity of the 337 keV line in band 8.

Levels $47/2^+$ *and* $45/2^-$. According to the level scheme of [1] level $43/2^-$ is fed by the cascade of $\gamma 508$ ($I_\gamma = 0.7$)and $\gamma 1089$ ($I_\gamma = 0.7$) transitions. They are not strong enough to

give the observed long-lived component, thus we suggest to add an additional unobserved transition connecting the long-lived level with level $43/2^-$, based on the level scheme [1]. In the DSA spectrum, a narrow lineshape of $\gamma 508$ indicates lifetimes of levels decaying by 508 keV transition as $\tau(\gamma 508) > 2$ ps. Analysis of $\gamma 1089$ and $\gamma 1084$ (band 8) observed in the DSA experiment at 143° gives evidence for $\sim 30\%$ side feeding of $\gamma 1089$. This allowed for a determination of $\tau(\gamma 1089)$ as $0.22(+0.16, -0.13)$ ps.

Level $43/2^-$. RDDSA analysis of the shape of $\gamma 608$ measured at 143° was performed for 4 distances, using the sum of the spectra gated on lines 337 and 462 keV. Taking into account feeding of level $43/2$ in accordance with Ref. [1], a large disagreement between τ values obtained from 608 keV spectra at different distances can be observed, pointing to the presence of a long-lived component feeding this level. Assuming the existence of feeding by a long-lived component with $\tau = 180 \pm 40$ ps, the agreement of τ value from different distances is reached under the condition that 40% of the intensity of $\gamma 608$ comes from the long-lived level.

Level $39/2^-$. Results of RDDSA analysis of $\gamma 1136$ are shown in Fig. 10. For this level $\tau = 1.9 \pm 1.0$ ps (including the error of intensity determination). The contribution of the long-lived component has been estimated as equal to 30% of full feeding of the level. In this case the stop component of the lineshape is mainly caused by the long-lived component. The bottom panel right shows the dependence of χ^2 on τ value of feeding transition.

4. Model calculations

4.1. The CQPC model

The low-lying negative-parity states in ^{119}I have a simple structure, based on the intruder $1h_{11/2}$ proton state placed high above the Fermi level (see below). This means that the properties of the negative-parity states in ^{119}I do not depend strongly on the position of the $h_{11/2}$ level, which is only approximately known from the Nilsson model calculation. This allows to drawn a reliable conclusion about the properties of the ^{119}I nucleus.

Negative-parity states in ^{119}I were analysed in the framework of the Core Quasi Particle Coupling (CQPC) model. The CQPC model (see [23,24] and also [5,25–27]) treats the states of the odd-A nucleus as a superposition of states in which:

(a) an odd particle is coupled to the $(A-1)$ even–even core,

(b) an odd hole is coupled to the $(A+1)$ even–even core.

The odd particle or hole are coupled to the core by the quadrupole–quadrupole interaction. The pairing interaction is also taken into account. A typical result of CQPC model calculation for negative-parity states based on the $1h_{11/2}$ particle located high above the Fermi level is presented in Fig. 11. Similar drawings for odd-A nuclei with rigid and gamma soft cores, can be found in Refs. [28] and [29], respectively. There is a very characteristic decoupled $\Delta I = 2$ band for the prolate shape of the core ($\gamma \leqslant 30°$) with spin sequence $11/2^-, 15/2^-, 19/2^-, \ldots$ and energy spacing approximately that of the core.

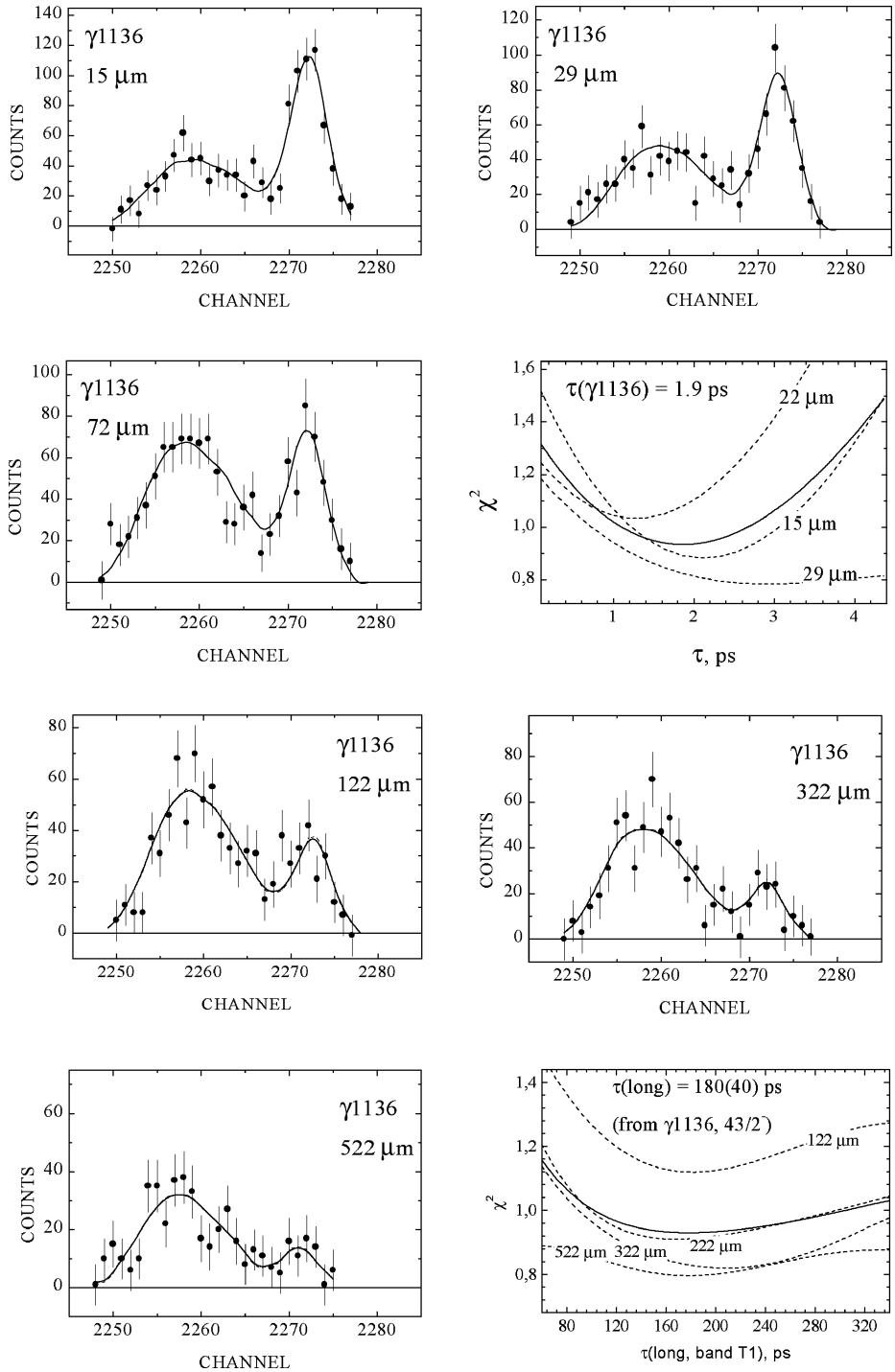

Fig. 10. RDDSA analysis of the 1136 line. See caption of Fig. 9.

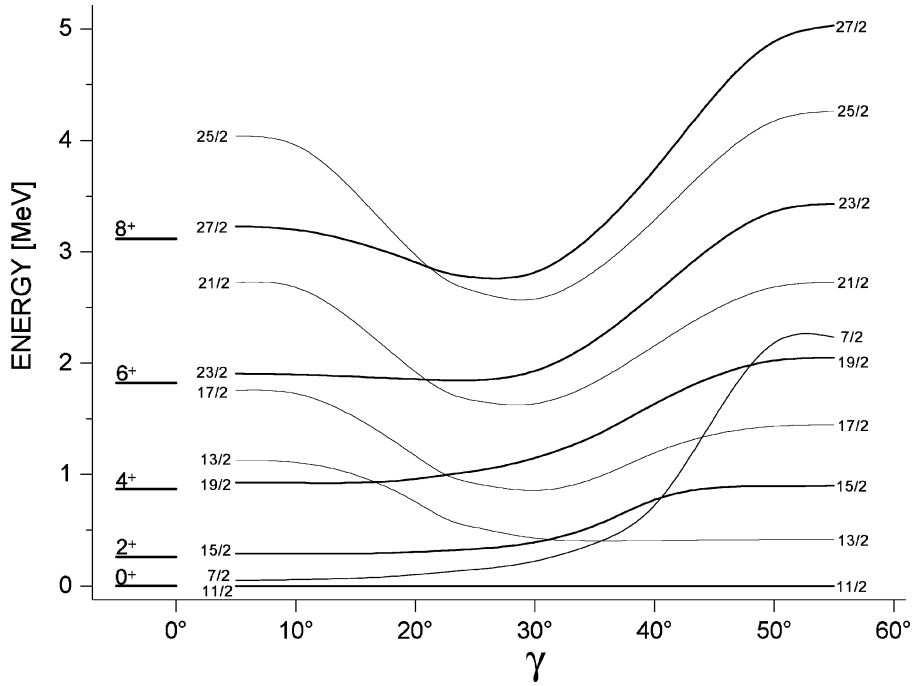

Fig. 11. Energy spectrum for an odd-A nucleus in which the $h_{11/2}$ nucleon (particle) is coupled to the rigid triaxial rotor described in the framework of the Davydov–Filippov model. The core parameters $E(2^+)$ and β are fixed. The left part of the figure presents the ground-state band of the even–even core ($\gamma = 0°$).

For the oblate shape ($\gamma > 30°$), some unfavored states become members of the strongly coupled $\Delta I = 1$ band with spin sequence $11/2^-$, $13/2^-$, $15/2^-$, $17/2^- \ldots$ The energy of the $7/2^-$ level placed (at $\gamma \approx 0°$) between $11/2^-$ and $15/2^-$ levels increases rapidly upon approaching $\gamma = 60°$.

Usually, real $(A-1)$ and $(A+1)$ nuclei can be treated as even–even cores. That is not the case for nuclei with Z or N close to a magic number. In such a case, the nuclear properties change rapidly and the cores differ significantly from real adjacent nuclei, due to the polarisation effect. Such a situation is found for the ^{119}I nucleus. Fig. 12 shows that the properties of ^{118}Te and ^{120}Xe are drastically different because of the proximity of the $Z = 50$ magic number. The energies of the decoupled band in ^{119}I follow the energies of the ground-state band in ^{120}Xe, rather than that in ^{118}Te. It seems that the $1h_{11/2}$ proton, added to ^{118}Te, changes the properties of the $(A-1)$ core, making it similar to ^{120}Xe. That is why, in the following, we will use the same data for description of $(A-1)$ and $(A+1)$ cores.

Spectroscopic information (spins R, excitation energies E_R, reduced matrix elements $\langle R||\mathrm{E2}||R'\rangle$ of the E2 operator) concerning even–even cores is needed as input data for the CQPC model. Presently, extensive information about the level scheme is available from experiments and can be taken as input data. However, information about the $\langle R||\mathrm{E2}||R'\rangle$ matrix elements is very scarce, especially concerning the diagonal reduced matrix elements

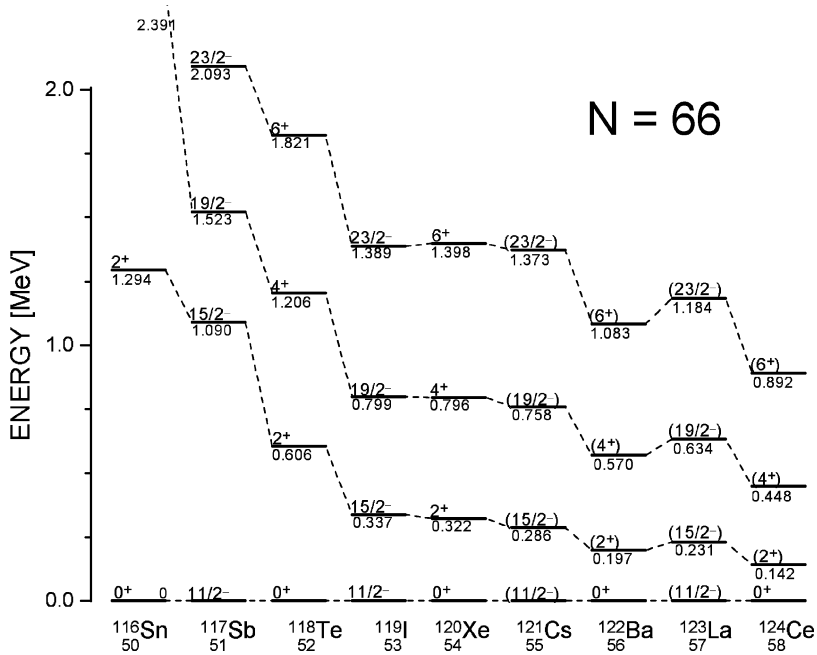

Fig. 12. Part of the level schemes of the ^{119}I and neighbouring nuclei with $N = 66$ [30,31]. Decoupled bands built on the $11/2^-$ state for odd-A nuclei are presented.

which are proportional to the spectroscopic electric quadrupole moments, and the signs of matrix elements which cannot be deduced from lifetime measurements. This difficulty can be overcome using theoretical models with parameters fitted to experimental data which give a large set of CQPC input data, indispensable for obtaining reliable results about properties of the odd-A nucleus.

To study the problem of γ-susceptibility, we applied two extreme nuclear models to describe core properties: the Wilets–Jean (W–J) model [32] for the γ-soft nucleus and the Davydov–Filippov (D–F) model [33,34] for the γ-rigid rotor. In the CQPC calculations, the 43 and 33 lowest states (up to maximal spin $R = 16^+$) were taken from the W–J and D–F models, respectively. The simplifying assumption was that properties R, E_R, $\langle R||\mathrm{E2}||R'\rangle$ of the $(A-1)$ and $(A+1)$ cores are the same. Single particle proton states (Fig. 13) were obtained from the spherical Woods–Saxon potential [35]. To describe the negative-parity levels in ^{119}I, the $1h_{11/2}$ and $2f_{7/2}$ states were considered. The most important contribution for the considered negative-parity states comes from the $1h_{11/2}$ state, the $2f_{7/2}$ state is of minor significance. For the pairing interaction the standard formula $\Delta = 135/A$ MeV was taken. The position of the Fermi level was fitted to reproduce the proper number of valence protons in ^{119}I. A quasiparticle–core coupling is described by a quadrupole–quadrupole interaction of strength as used in previous works for the $50 < Z$, $N < 82$ mass region [25–27]. To calculate the electromagnetic properties of ^{119}I, we applied the bare proton charge ($e_{\mathrm{eff}} = e_{\mathrm{free}}$), the standard orbital g-factor ($g_p^{(l)} = 1$) and effective spin g-factor $g_{\mathrm{eff}}^{(\mathrm{s})} = 0.6 g_{\mathrm{free}}^{(\mathrm{s})}$.

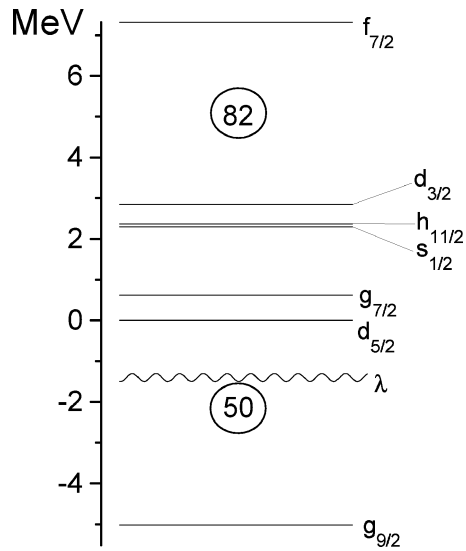

Fig. 13. Single-particle proton states taken into account in the present calculations. λ is the position of the Fermi level.

4.2. The γ-soft core of the ^{119}I nucleus

To describe the γ-soft core for the ^{119}I nucleus, the Wilets–Jean model was used in the extended version given by Dobaczewski et al. [36]. The following approximations were made:

(a) the rotational inertial functions $B_x = B_y = B_z = B_{\gamma\gamma} = B = \text{const}$,
(b) the vibrational inertial functions $B_{\beta\beta} = \text{const}$, whereas $B_{\beta\gamma} = 0$,
(c) the potential energy surface (PES) is gamma-independent (which reproduces results of microscopic calculations for transitional nuclei) and reads:

$$V(\beta) = \frac{1}{2}C_2\beta^2 + C_8\beta^8 + G\left[\exp\left(-\frac{\beta^2}{a^2}\right) - 1\right]. \tag{5}$$

The Wilets–Jean model (with $C_8 = 0$) fitted to ^{120}Xe energy levels does not give a satisfactory enough reproductions of experimental data. To obtain better agreement with the experimental B(E2) values in ^{120}Xe as well as in ^{119}I we introduced a large value of C_8. To reproduce the level scheme of ^{119}I, we had to increase the values of the inertial functions. The W–J model parameters were as follows: $C_2 = 0.01$ MeV, $C_8 = 1.5 \times 10^4$ MeV, equilibrium deformation $\beta_\circ = 0.276$, the depth of potential $D = V(\beta_\circ = 0) - V(\beta_\circ) = 7.6$ MeV, $B = 110\,\hbar^2/\text{MeV}$, $B_{\beta\beta} = 10^3\,\hbar^2/\text{MeV}$. Fig. 14 and Table 3 compare the properties of this and other cores with the real ^{120}Xe nucleus.

4.3. The γ-rigid cores of the ^{119}I nucleus

To investigate the possibility of describing the ^{119}I nucleus by the γ-rigid core model, the Davydov–Filippov model with different sets of parameters was used. Model

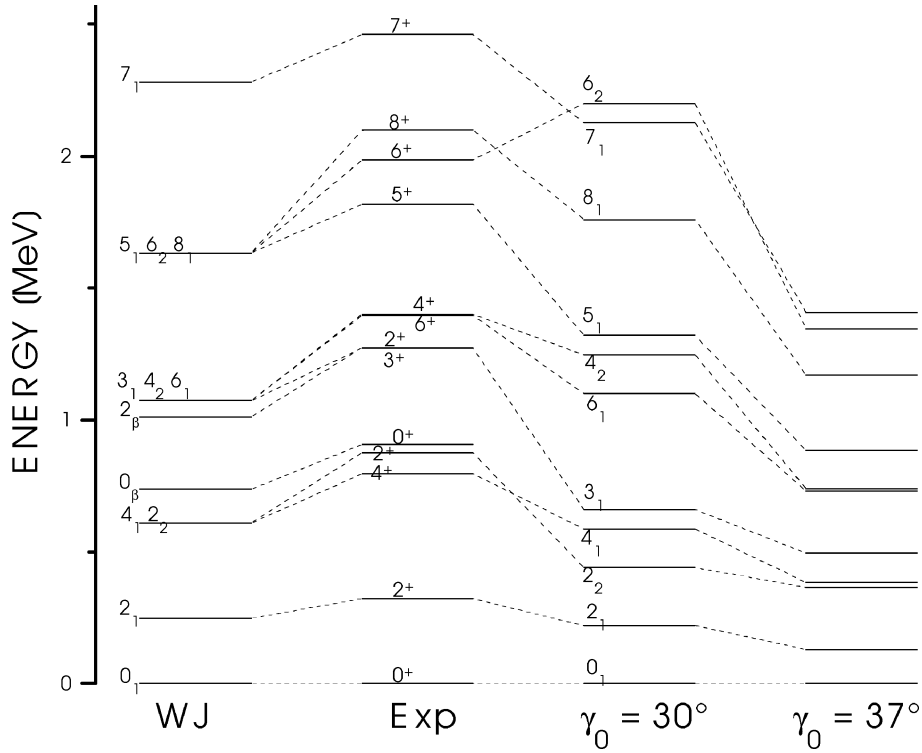

Fig. 14. The low-lying states of ^{120}Xe [37] compared with the level scheme calculated using the γ-soft core (W–J) and γ-rigid cores with different $\gamma_\circ$ (variants: DF-B, DF-C). DF-A is not shown because the experimental energies of ^{120}Xe levels were used in CQPC calculation.

Table 3
Reduced transition probabilities B(E2) in the ^{120}Xe nucleus. The experimental values [38] are compared with calculated ones in the γ-soft (W–J) and γ-rigid (D–F, different $\gamma_\circ$ according to A, B and C variants) models. The B(E2) values are given in e^2b^2 units

Transition	W–J	exp	DF-A, $\gamma_\circ = 23.4°$	DF-B, $\gamma_\circ = 30°$	DF-C, $\gamma_\circ = 37°$
$2^+ \to 0^+$	0.31	0.36 ± 0.03	0.36	0.39	0.43
$4^+ \to 2^+$	0.45	0.42 ± 0.04	0.51	0.54	0.64
$6^+ \to 4^+$	0.54	0.44 ± 0.05	0.61	0.68	0.81

parameters, namely $\beta_\circ$ and $\gamma_\circ$ and the energy $E(2_1^+)$ of the first 2^+ state, are listed in Table 4. The properties of these cores are compared with experimental data for ^{120}Xe in Fig. 14 and Table 3. The following three variants of the Davydov–Filippov model are considered:

DF-A — the properties of the core follow real ^{120}Xe,

DF-B — the parameter $\gamma_\circ = 30°$, which corresponds to $\langle\gamma\rangle = 30°$ in the γ-soft core

Table 4
Parameters for rigid cores

Variant	DF-A	DF-B	DF-C
$\gamma_\circ$	23.4°	30°	37°
$\beta_\circ$	0.29	0.31	0.36
$E(2^+)$ (keV)	322.4	200	130

(described in the previous section). The rest of the parameters were adjusted to reproduce ^{119}I,

DF-C — all parameters were adjusted to reproduce the properties of ^{119}I, particularly transition probabilities in band 9.

In variant A, the parameter $\beta_\circ = 0.289$ was obtained from the experimental value of the lifetime $\tau(2_1^+) = 64$ ps [38], whereas the asymmetry parameter, $\gamma = 23.4°$ was derived from the experimental value of the ratio $E(2_2^+)/E(2_1^+) = 2.72$ [37]. Such a γ-deformation parameter for ^{120}Xe agrees with the systematics for the neighbouring Xe nuclei [39]. The experimental energies of the ^{120}Xe nucleus were taken as input data for the CQPC model calculation. When the experimental energy for spin R was not available, a calculated one was taken. The following procedure was used: the ratio, $E^{\text{theory}}(R)/E^{\text{exp}}(R)$ of the calculated energy (from the D–F model) to the experimental one, can be approximated [40] by the equation:

$$E^{\text{theory}}(R)/E^{\text{exp}}(R) = a \cdot E^{\text{theory}}(R) + b. \tag{6}$$

Parameters a and b, identical for all spins, were determined from a fitting procedure.

With respect to variants B and C, one can see from Fig. 11 that the energy of levels $15/2^-$, $19/2^-$, ... increases rapidly when $\gamma_\circ > 30°$. Thus, to reproduce ^{119}I, the energies of the core states have to be substantially reduced (compare $E(2_1^+) = 322$ keV in the real ^{120}Xe nuclei with $E(2_1^+) = 200$ and 130 keV in cases B and C). It is equivalent to a large increase of the moment of inertia for variants B and C.

4.4. Comparison of model calculations with experiment

The results of model calculation for ^{119}I are compared with experimental energy levels and B(E2) transition probabilities in Figs. 15,16 and Table 5.

The results of calculations using γ-rigid cores are as follows:

– In variant DF-A, parameters of the core were chosen to reproduce ^{120}Xe. Reasonable agreement with experimental data was obtained for bands 6 and 8; band 7 is predicted too high in energy in the calculations. Band 9 is less regular than it is observed in the experiment. Theoretical calculations predict $B(\text{E2}; 11/2^- \to 7/2^-)$ value several times smaller than the one obtained in the experiment. Calculations also predict strong

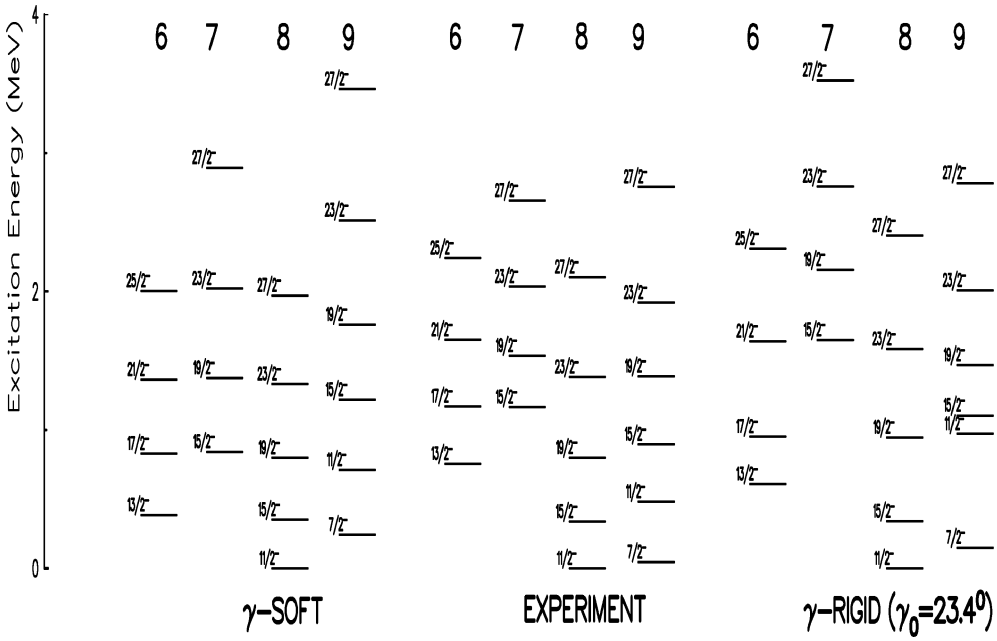

Fig. 15. Negative-parity states in ^{119}I. The experimental level scheme (bands 6–9) [1] is compared with the results of the CQPC model calculations. "SOFT" and "RIGID" refer to calculations for γ-soft ($\langle\gamma\rangle = 30°$) and γ-rigid ($\gamma_\circ = 23.4°$) cores.

transition from the $11/2^-$ level belonging to band 9 to a $9/2^-$ level. Such a decay is not observed and the $9/2^-$ level is not visible in the experiment.

– In variant DF-B we made an attempt to describe the experimental data assuming γ-rigid core with a fixed asymmetry parameter, $\gamma_\circ = 30°$, which corresponds to $\langle\gamma\rangle = 30°$ of the γ-soft core. Disagreement with the experiment is observed in band 9. Theory gives irregular spacing between levels and too low B(E2) value for the $11/2^- \to 7/2^-$ transition. Calculations also predict an M1 transition, $11/2^- \to 9/2^-$, of energy about 295 keV, 8 times more intense than the $11/2^- \to 7/2^-$ E2 transition. Such a 295 keV transition, or any similar energy one is not observed although its predicted intensity is more than 10 times stronger than our detection limit.
– In variant DF-C it was found that the energy levels and electromagnetic properties of band 9 are better reproduced for $\gamma_\circ = 37°$ than in variants DF-A and DF-B (see Fig. 16 and Table 5). However, band 6 becomes so much lower, that it creates together with band 8 a strongly coupled $\Delta I = 1$ band structure not observed in the experiment. This effect, discussed in Section 4.1, can be seen in Fig. 11 where the strongly coupled band becomes visible for $\gamma_\circ \to 60°$. A similar strongly coupled structure is predicted for band 9: $7/2^-$, $9/2^-$, $11/2^-$, $13/2^-$, $15/2^-$, $17/2^-$ and $19/2^-$ with strong $\Delta I = 1$ transitions. The predicted intense M1 transition $11/2^- \to 9/2^-$, of an energy of 208 keV or any similar energy is not observed although its expected intensity is more

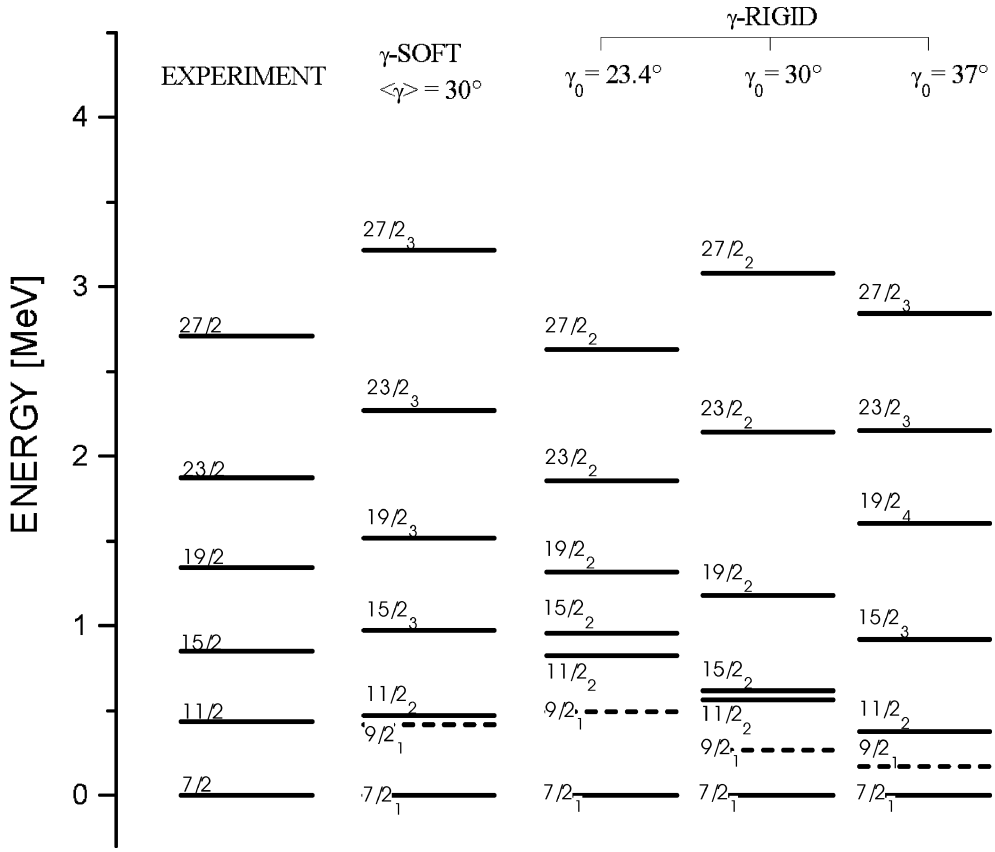

Fig. 16. Level scheme of the band 9. The experimental data are compared with their theoretical counterparts calculated with the γ-soft ($\langle\gamma\rangle = 30°$) and γ-rigid ($\gamma_\circ = 37°$, 30° and 23.4°) cores. In all cases the energy of the $7/2^-$ state is set at zero. The $9/2^-$ levels not seen in experiment are shown as dashed lines.

than 30 times stronger than our detection limit. It is worthwhile to stress that in variant DF-C an abnormally large moment of inertia was assumed (see value of $E(2_1^+)$ in Table 4). It means that one proton added to ^{118}Te ($Z = 52$) should polarize the core of ^{119}I ($Z = 53$) stronger then 6 protons in ^{124}Ce ($Z = 58$) — see Fig. 12.

For the γ-soft core, the calculations reproduce the level structure and inband B(E2) transition probabilities for all the bands, also $B(\mathrm{E2}; 11/2^- \to 7/2^-)$ for band 9. Regarding the $11/2^- \to 9/2^-$ transition the W–J model predicts energy of 51 keV and an intensity many times smaller than our detection limit. In the calculation the bandheads 6 and 7 are too low and bandhead 9 is too high. It is probably due to oversimplification of the considered version of the γ-soft model (with γ-independent inertial functions and potential energy surface) and can be corrected by a small shift from $\langle\gamma\rangle = 30°$ towards prolate shape. This shift increases the energy of the $13/2$ state and decreases the energy of the $7/2$ level as is seen in Fig. 11.

Table 5
Experimental and theoretical values of B(E2) (in e^2b^2 units) for the negative-parity states in ^{119}I

$I_i \to I_f$	Experiment	γ-soft W–J	$\gamma_o = 23.4°$ DF-A	$\gamma_o = 30°$ DF-B	$\gamma_o = 37°$ DF-C
Band 9					
$27/2 \to 23/2$	0.31 (+0.09, −0.06)	0.41	0.47	0.45	0.30
$23/2 \to 19/2$	0.24 (+0.05, −0.04)	0.32	0.45	0.24	0.34
$19/2 \to 15/2$	0.28 (+0.04, −0.03)	0.17	0.46	0.30	0.24
$15/2 \to 11/2$	0.34 (+0.05, −0.04)	0.28	0.43	0.35	0.24
$11/2 \to 7/2$	0.15 (+0.04, −0.03)	0.17	0.04	0.07	0.11
Band 8					
$27/2 \to 23/2$	0.49 (+0.10, −0.07)	0.68	0.62	0.72	0.81
$23/2 \to 19/2$	0.48 (+0.09, −0.06)	0.62	0.57	0.52	0.66
$19/2 \to 15/2$	0.49 (+0.05, −0.04)	0.50	0.50	0.37	0.33
$15/2 \to 11/2$	0.41 (+0.03, −0.03)	0.33	0.46	0.37	0.35
Band 7					
$27/2 \to 23/2$	0.59 (+0.15, −0.10)	0.48	0.57	0.29	0.52
$23/2 \to 19/2$	0.29 (+0.10, −0.06)	0.43	0.56	0.18	0.37
Band 6					
$25/2 \to 21/2$	0.62 (+0.12, −0.09)	0.59	0.61	0.63	0.74
$21/2 \to 17/2$	0.64 (+0.22, −0.16)	0.48	0.55	0.52	0.54

5. Summary

Unique information about electromagnetic properties of four negative-parity bands, originating from the $h_{11/2}$ quasiproton coupled to an axially asymmetric core, was obtained. This was possible since:

(i) the improved joint analysis of the DSA and RDM data was employed;
(ii) the most important contributions of experimental inaccuracy were substantially reduced by the self-calibration of stopping power formula parameters.

The lifetimes of 31 negative-parity levels were determined. That is one of the largest sets of electromagnetic transition probabilities (Fig. 5) for an odd-A nucleus from the $50 < Z, N < 82$ region yet obtained.

The experimental data presented in this paper and in Ref. [1] allow us to draw a conclusion concerning the shape of the ^{119}I nucleus. We see that the 53rd proton added to the ^{118}Te nucleus, through the polarization effect, changes the properties of the even–even core. The β-deformation becomes at least as large as that of ^{120}Xe ($\beta \approx 0.28$), whereas the γ-deformation is around 30°. Comparison of experimental data with theoretical calculations indicates the advantage of the γ-soft model over the γ-rigid one in the description of $h_{11/2}$ band structure in ^{119}I. These conclusions agree with the results of microscopic calculations [4], according to which the transitional nuclei from the mass region being considered are γ-soft with an average value of the γ-deformation close to 30°.

One can see, that the most valuable information concerning the shape of ^{119}I is based on the properties of the unfavoured states, especially those belonging to band 9, with their

regular energy spacing and fast intraband transitions. It is worthwhile to mention that bands 9 and 7 were not well reproduced in the framework of the cranking shell model calculation [1].

Acknowledgements

This work was partially supported by Polish State Committee for Scientific Research (KBN) (contract No. 2P302 151 06). We are grateful to the staff of Niels Bohr Institute. We would like also thank to the Academy of Finland, the Danish Natural Science Research Council, NORDBALL collaboration and the Mianowski Kasa foundation. Thanks are given to Dr. R. Kaczarowski for stimulating discussion concerning interpretation of our data. Software written by D.C. Radford was used in the data analysis. Thanks are given to Prof. Zaleski for hospitality given to one of us (A.A.P.) during stay in Warsaw.

Appendix A

The aim of this appendix is to discuss the influence of the deorientation effect on lifetimes measured by the Recoil Distance Method. Let us consider the decay of a single level. Then $S_u/S = \exp(-t_D/\tau)$ where S_u and S_s are intensity of unshifted and shifted components of the γ-line, respectively, $S = S_u + S_s$, t_D — time of flight of the recoil over distance D between target and stopper, τ — lifetime of the level under investigation. In this simple case, experimentally extracted τ value is independent of D and defined as $\tau = t_D/\ln(S/S_u(D))$. Deorientation affects $S^d(D)$ and $S_u^d(D)$ and thus the measured τ^d-value depends on D and $\tau^d = t_D/\ln(S^d(D)/S_u^d(D))$. Induced by the effect of deorientation, the relative error of measured lifetime $\Delta\tau(D)$ is a function of the distance D:

$$\Delta\tau(D)/\tau^d = 1 - \tau/\tau^d = 1 - \tau\ln\bigl(S^d(D)/S_u^d(D)\bigr)/t_D. \tag{7}$$

According to the Abragam–Pound paper [41], an angular distribution of γ-rays $W(t,\Theta)$, under the assumption that $A_4P_4(\Theta)$ is small, is modified for γ-quantas emitted when the recoil travels through vacuum:

$$W(t,\Theta) = 1 + A_2P_2(\Theta)\exp(-t/\tau_2),$$

where τ_2 is the deorientation characteristic time. For the stopped component of the γ-line, $W(t,\Theta)$ is "frozen" at the $W(t_D,\Theta)$ value. Then

$$\begin{aligned}
S_u^d(D) &= C\exp(-t_D/\tau)\bigl(1 + A_2P_2(\Theta)\exp(-t_D/\tau_2)\bigr),\\
S_s^d(D) &= C1/\tau\int_0^{t_D}\exp(-t/\tau)\bigl(1 + A_2P_2(\Theta)\exp(-t/\tau_2)\bigr)\,\mathrm{d}t,\\
S^d(D) &= C\bigl(1 + A_2P_2(\Theta)\bigl(\exp(-t_D/\tau_2 - t_D/\tau)\\
&\qquad + \bigl(1 - \exp(-t_D/\tau_2 - t_D/\tau)\bigr)/(1 + \tau/\tau_2)\bigr)\bigr),
\end{aligned}$$

where C is a constant.

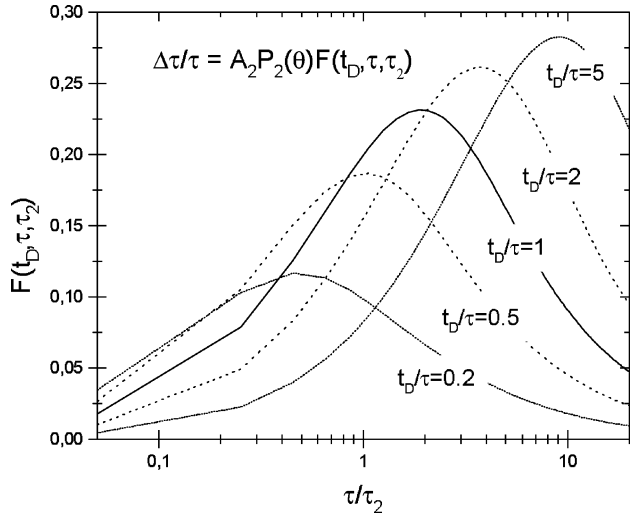

Fig. A.1. Deorientation error factor F as a function of characteristic deorientation time τ_2, measured lifetime τ and time of flight of the recoil t_D.

From Eq. (7), using first order approximation of the $\ln(1+x)$ function we obtain:

$$\Delta\tau/\tau^d = A_2 P_2(\Theta) F(\alpha,\beta), \quad \text{where } \alpha = \tau/\tau_2, \beta = t_D/\tau \quad \text{and}$$
$$F(\alpha,\beta) = \big(\exp(-\alpha\beta) - 1 + \alpha\big(1 - \exp(-\beta - \alpha\beta)/(1+\alpha)\big)\big)/\beta.$$

As one can see from Fig. A.1, in the lineshape analysis, the error of τ due to vacuum deorientation is small. This is due, in part, to the fact that shifted and unshifted components both change in the same direction (for an independently normalized unshifted peak, the error is larger). In cases discussed in this paper, $A_2 \approx 0.3 \div 0.4$, $P_2(143^\circ) = 0.45$, $F \approx 0.1 \div 0.2$. Then, typical errors in lifetime determination are $\approx 2 \div 3\%$.

References

[1] S. Törmänen, S. Juutinen, R. Julin, A. Lampinen, E. Mäkelä, M. Piiparinen, A. Savelius, A. Virtanen, G.B. Hagemann, Ch. Droste, W. Karczmarczyk, T. Morek, J. Srebrny, K. Starosta, Nucl. Phys. A 613 (1997) 282.
[2] J. Adam, M. Honusek, A. Spalek, D.N. Dojnikov, A.D. Efimov, M.F. Kudojarov, I.Kh. Lemberg, A.A. Pasternak, O.K. Vorov, U.Y. Zhovliev, Z. Phys. A 332 (1989) 143.
[3] S.G. Rohoziński, J. Srebrny, K. Horbaczewska, Z. Phys. 268 (1974) 401.
[4] S.G. Rohoziński, J. Dobaczewski, B. Nerlo-Pomorska, K. Pomorski, J. Srebrny, Nucl. Phys. A 292 (1977) 66.
[5] Ch. Droste, D. Chlebowska, J. Dobaczewski, F. Dönau, A. Kerek, G. Leander, J. Srebrny, W. Waluś, Nucl. Phys. A 341 (1980) 98.
[6] N.V. Zamfir, R.F. Casten, Phys. Let. B 260 (1991) 265.
[7] I.Kh. Lemberg, A.A. Pasternak, Modern Methods of Nuclear Spectroscopy, Nauka, Leningrad, 1985.
[8] Yu.N. Lobach, A.A. Pasternak, J. Srebrny, Ch. Droste, G.B. Hageman, S. Juutinen, T. Morek, M. Piiparinen, E.O. Podsvirova, S. Törmanen, K. Starosta, A. Virtanen, A.A. Wasilewski, Acta Phys. Pol. B 30 (1999) 1273.

[9] I.Kh. Lemberg, A.A. Pasternak, Nucl. Instrum. Methods 140 (1977) 71.
[10] M.C. Bertin, N. Benczer-Koller, G.G. Seaman, J.R. MacDonald, Phys. Rev. 183 (1969) 964.
[11] I. Lindhard, V. Nielsen, M. Scharff, Dan. Vidensk. Selsk. Mat. Fys. Medd. 36 (1968) 10.
[12] I. Lindhard, M. Scharff, H.E. Schiott, Dan. Vidensk. Selsk. Mat. Fys. Medd. 33 (1963) 1.
[13] R. Schwengner, G. Winter, J. Döring, L. Funke, P. Kemnitz, E. Will, A.E. Sobov, A.D. Efimov, M.F. Kudojarov, I.Kh. Lemberg, A.S. Mishin, A.A. Pasternak, L.A. Rassadin, I.N. Chugunov, Z. Phys. A 326 (1987) 287.
[14] M.F. Kudojarov, I.Kh. Lemberg, A.S. Mishin, A.A. Pasternak, L.A. Rassadin, in: 31 Conf. on Nuclear Spectr. and Structure, 1981, p. 411.
[15] G. Winter, F. Dubbers, J. Döring, L. Funke, P. Kemnitz, E. Will, D.S. Andreev, K.I. Erochina, I.Kh. Lemberg, A.A. Pasternak, J. Phys. G 11 (1985) 277.
[16] I.N. Vishnevsky, E.V. Kuzmin, M.F. Kudojarov, Yu.N. Lobach, A.A. Pasternak, I.P. Tkachuk, V.V. Trishin, Ukr. Phys. J. 33 (1988) 608.
[17] C.D. Moak, M.D. Brown, Phys. Rev. 149 (1966) 244.
[18] F. Ziegler, J.P. Biersack, U. Littmark, The Stopping Powers and Ranges of Ions in Matter, Vol. 1, Pergamon, New York, 1985.
[19] J. Urbon, D.G. Sarantites, L.L. Rutledge, Nucl. Instrum. Methods 126 (1975) 49.
[20] H.P. Hellmeister, K.P. Lieb, W. Muller, Nucl. Phys. A 307 (1978) 515.
[21] A.A. Pasternak et al., Eur. Phys. J. A, submitted.
[22] P. Petkov, J. Gableske, O. Vogel, A. Dewald, P. von Brentano, R. Krücken, R. Peusquens, A. Nicolay, A. Gizon, J. Gizon, D. Bazzacco, C. Rossi-Alvarez, S. Lunardi, P. Pavan, D.R. Napoli, W. Andrejtscheff, R.V. Jolos, Nucl. Phys. A 640 (1998) 293.
[23] F. Dönau, S. Frauendorf, Phys. Lett. B 71 (1977) 263.
[24] F. Dönau, U. Hagemann, Z. Phys. A 293 (1979) 31.
[25] K. Starosta, Ch. Droste, T. Morek, J. Srebrny, D.B. Fossan, S. Gundel, J.M. Sears, I. Thorslund, P. Vaska, M.P. Waring, S.G. Rohoziński, W. Satula, U. Garg, S. Naguleswaran, J.C. Walpe, Phys. Rev. C 55 (1997) 2794.
[26] Ch. Droste, T. Morek, S.G. Rohoziński, D. Alber, H. Grave, D. Chlebowska, J. Phys. G 18 (1992) 1763.
[27] T. Morek, K. Starosta, Ch. Droste, D. Fossan, G. Lane, J. Sears, J. Smith, P. Vaska, Eur. Phys. J. A 3 (1998) 99.
[28] J. Mayer-ter-Vehn, Nucl. Phys. A 249 (1975) 111 and 141.
[29] G. Leander, Nucl. Phys. A 273 (1976) 286.
[30] R.B. Firestone, Table of Isotopes, 8th ed., Wiley, New York, 1996.
[31] K.L. Ying, P.J. Bishop, A.N. James, A.J. Kirwan, D.J.G. Love, T.P. Morrison, P.J. Nolan, D.C.B. Watson, K.A. Conell, A.H. Nelson, J. Simpson, J. Phys. G 12 (1986) L211.
[32] L. Wilets, M. Jean, Phys. Rev. 102 (1956) 788.
[33] A.S. Davydov, G.F. Filippov, Nucl. Phys. 8 (1958) 237.
[34] J.M. Eisenberg, W. Grainer, Nuclear Models, Nuclear Theory, Vol. 1, North-Holland, Amsterdam, 1970.
[35] S. Ćwiok, W. Dudek, private communication.
[36] J. Dobaczewski, S.G. Rohoziǹski, J. Srebrny, Z. Phys. A 282 (1977) 203.
[37] S. Törmanen, S. Juutinen, R. Julin, B. Cederwall, A. Johnson, R. Wyss, P. Ahonen, B. Fant, M. Matsuzaki, J. Nyberg, M. Piiparinen, A.S. Mitarai, J. Mukai, A. Virtanen, Nucl. Phys. A 572 (1994) 417.
[38] J.C. Walpe, B.F. Davis, S. Naguleswaran, W. Reviol, U. Garg, Xing-Wang Pan, Da Hasuan Feng, J.X. Saladin, Phys. Rev. C 52 (1995) 1792.
[39] J. Yan, O. Vogel, P. von Brentano, A. Gelberg, Phys. Rev. C 48 (1993) 1046.
[40] A.A. Wasilewski, MSc Thesis, Warsaw University, 1998.
[41] A. Abragam, R.V. Pound, Phys. Rev. 92 (1953) 943.